MICROSTRUCTURAL INFLUENCE ON TENSILE AND FATIGUE PROPERTIES OF TI6AL4V (ELI) PRODUCED THROUGH DIRECT METAL LASER SINTERING

N.M. Baloyi[1*], P. Mendonidis[1], W. Du Preez[2] & A.P.I. Popoola[3]

[1*]Department of Metallurgical Engineering, Vaal University of Technology, South Africa, nkeleb@vut.ac.za, peter@vut.ac.za

[2]Department of Mechanical and Mechatronics Engineering, Central University of Technology, South Africa,wdupreez@cut.ac.za

[3]Department of Chemical, Metallurgical and Materials Engineering, Tshwane University of Technology, South Africa, PopoolaAPI@tut.ac.za

ABSTRACT

Microstructure of Ti6Al4V (ELI) components manufactured in two orientations (Vertical-Z and Horizontal-X) from direct metal laser sintering (DMLS) were transformed to equiaxed (Z) and lamellar (X) by heat treatment below the beta transus at 950ºC. The hardness, tensile and fatigue properties showed direction correlation; with vertically built (~843 MPa) samples having lower tensile properties than the horizontal samples (~895 MPa). However, the fatigue properties favoured the lamellar microstructure over the bimodal microstructures.

1 INTRODUCTION

Ti6Al4V extra low interstitial (ELI), or grade 23, has a low content of impurities such as oxygen, nitrogen, and carbon. Due to improved mechanical properties, biocompatibility and corrosion properties, this alloy is continuously used as a replacement of hard tissues (e.g. femoral stem) [1]. Unfortunately, not everything about Ti6Al4V is advantageous. Reports on prostheses failure of the alloy are published regularly, such as [1,2,3]. Most premature failures are directly related to component fatigue properties.

Microstructure in metals defines properties such as tensile strength, fatigue and toughness. With Ti6Al4V (ELI) the α + ß arrangement controls microstructure transformation depending on the heat treatment employed [4]. These methods are known as: (1) cooling from the β phase-field or (2) recrystallization and globularisation process, yielding lamellar or equiaxed microstructures, respectively . Lamellar microstructures as reported by [5] are characterised by lower strength, lower ductility and better fatigue propagation when they are compared to equiaxed microstructure [5]. This is because lamellar structures have a greater α/ß surface and more oriented colonies which delay the crack initiation stage, while the equiaxed type is dominated by primary α grains which stimulate coalesce of micro-cracks [6,7].

Failure of material under fluctuating stresses at a stress magnitude which is lower than the ultimate tensile strength of the material is called fatigue failure. The contributing stresses to fatigue failure are low and the failure process consists of: (1) crack nucleation, crack growth and (3) final fracture (Figure 1). This indicates that metals fatigue properties are either crack initiation or crack propagation controlled. The nature of the process involves cyclic motions that subject metal components to atomic deformation which could result in micro-plastic deformation [8]. Cracks could initiate at the surface due to the micro-plastic deformation propelled by high-stress concentration near the surface. Another way of crack initiation could be from the impurities, pores and/or inclusions within the area of the metal, especially produced through DMLS [9].

*Corresponding author

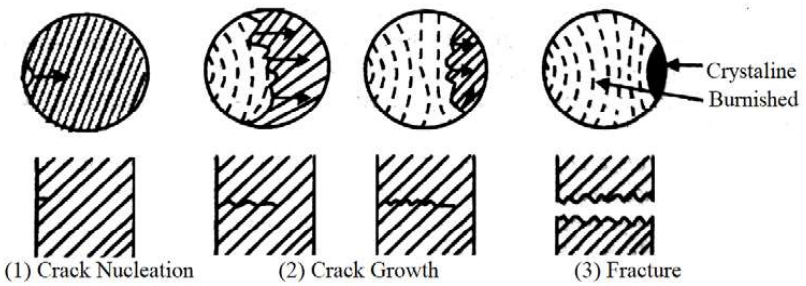

Figure 1: Stages of fatigue [10]

Characterisation of fatigue properties of components built through DMLS used in the biomedical application is continuously improving; specifically, to reduce the reports on failing Ti6Al4V prostheses [1]. DMLS is ideal to produce customised components and saving of material. Challenges with the process include porosity, from the layer by layer fashion built and uncontrolled microstructure [10]. These two setbacks increase the difficulty to understand fatigue properties of Ti6Al4V (ELI). Therefore, this investigation aims at investigating the influence of microstructure on the fatigue properties when DMLS components are built at different orientations.

2 METHODOLOGY

Blank rectangular blocks of length (*l*) 12 mm, width (*w*) 12mm and height (*h*) 75 mm were produced from Ti6Al4V ELI powder via an EOS M280 machine. They were produced along both vertical (Z) and horizontal (X) build direction. Processing parameters such as; laser power: 170 W, spot diameter: 80 µm, scanning speed: 1200 mm/s, hatch spacing: 0.1 mm, layer thickness: 30 µm, build rate: 3.75 mm^3/s and the part density: 4.41 g/cm^3, were kept constant. Layers were built in a zigzag scanning pattern which was changing with scanning direction at 67° from layer to layer. The chemical composition of the powder, both as specified by the supplied (TLS Technik GmbH) and the laboratory analysed varied within the acceptable limits of the ASTM F3001 (Table 1). The average particle size of 26 µm and 90% passing at 37 µm, which promote consistent building rate.

Table 1: Powder chemical properties

	ASTM F3001 / F136	*Supplier*	*Analysed [11]*	*Reused [11]*
Elements	*Composition (%)*	*Composition (%)*	*Composition (%)*	*Composition (%)*
Nitrogen	0.05	0.006	0.018 - 0.022	0.014 - 0.021
Carbon	0.08	0.016	---	---
Hydrogen	0.012	0.002	---	---
Yttrium	0.005	<0.001	---	---
Iron	0.25	0.25	0.16 - 0.17	0.16 - 0.23
Oxygen	0.13	0.082	0.11 - 0.12	0.11 - 0.12
Aluminum	5.5 - 6.5	6.34	5.93 - 6.04	5.85 - 6.15
Vanadium	3.5 - 4.5	3.94	3.84 - 3.92	3.91 - 4.07
Titanium	balance	Balance	90	90

It is common for DMLS produced Ti6Al4V ELI parts to pass through post processing treatments such as stress relieve and annealing. Stress relieve treatment was done at 650 °C for 4 h in an argon furnace to reduce the oxidation of Ti6Al4V ELI. This was to remove stresses induced by the layer manufacturing, and to successfully remove the parts off the building platform without deformation. To homogenise the mechanical properties, high temperature annealing (HTA) was employed at 950 °C in a vacuum atmosphere furnace, and cooling was done in the $\alpha + \beta$ region. This process helped

to decompose the needle type acicular α' martensitic microstructure from the DMLS fast cooling behaviour.

To meet the mechanical testing standards, samples were machined following ASTM E8 and ASTM E466 for tensile and fatigue specifications, respectively. Tensile testing was performed using a 1342 Instron servo hydraulic testing machine equipped with a class B1 extensometer on a 25 mm gauge length with a 4.4 mm gauge diameter specimen. Fatigue life was set at 2 million cycles on a constant amplitude load control using a sinusoidal wave form at a frequency of 10 Hz and a load ratio (R-ratio) of 0.1. The applied load was estimated from the ultimate tensile strength data and was between 650 MPa - 540 MPa load. The microstructure and fractography were observed using optical microscopy (OM) and scanning electron microscopy equipped with energy dispersive spectroscopy (SEM/EDS).

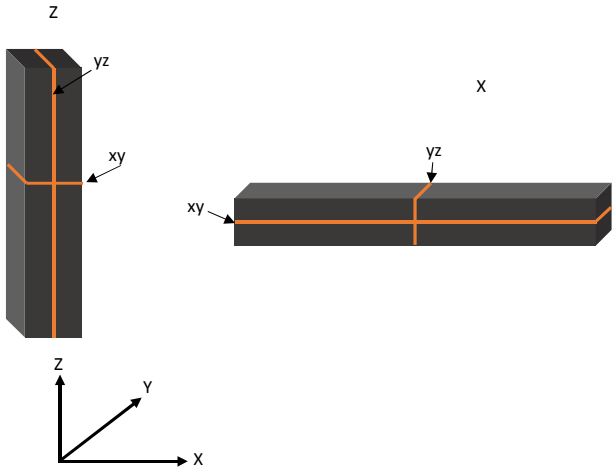

Figure 2: Hardness sectioning and indentation procedure

The hardness of the material was measured using the Vickers microhardness method. The samples were sectioned to evaluate the difference between build direction and scanning pattern hardness values following the procedure demonstrated in Figure 2. Six/eight (depending on the dimensions of the sample) consecutive indentation points at a distance of 150 µm where achieved using a 1000g load for 15 seconds dwelling; to fulfil the parameters of equation (1).

$$HV = \frac{1.854F}{d^2} \quad \text{.....1)}$$

3 RESULTS AND DISCUSSION

3.1 Microstructure analysis and Vickers hardness measurement

Microstructures were investigated in order to measure the success of the HTA heat treatment. Ti6Al4V ELI manufactured by DMLS have microstructural instability induced by the fast cooling nature from the process [12]; besides, the alloy is a mixture of two phases (α + β). Ti4Al4V ELI produced from DMLS is primarily composed of acicular α' martensitic microstructure which influences the fatigue properties negatively. Therefore, transformation is done to attain specific morphology,

size and texture of the constituent phases [6]. HTA is introduced to decompose this α' → α and from α → β which endorse equiaxed or duplex microstructures [9].

Figure 3 illustrates the microstructure observed from the two samples (Z and X). Figure 3 (a & b) show the SEM microstructures with Z-xy view resembling the equiaxed type while the X-yz type microstructure are similar to lamellar. The figure shows the different in concentration of the white /dark phases. The white phases are denoted β - phase while the dark phases as the α - phase. The equiaxed microstructure have a fair distribution of the phases than the X type which shows longer lath. This is common, as the equiaxed is the β containing microstructure than the lamella; which are α lath dominated.

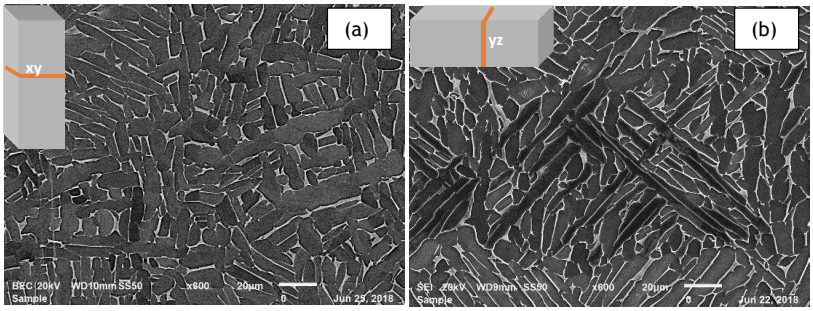

Fig. 3: SEM microstructure of (a) vertically (Z) grown, xy view; (b) horizontal (X) grown, yz view.

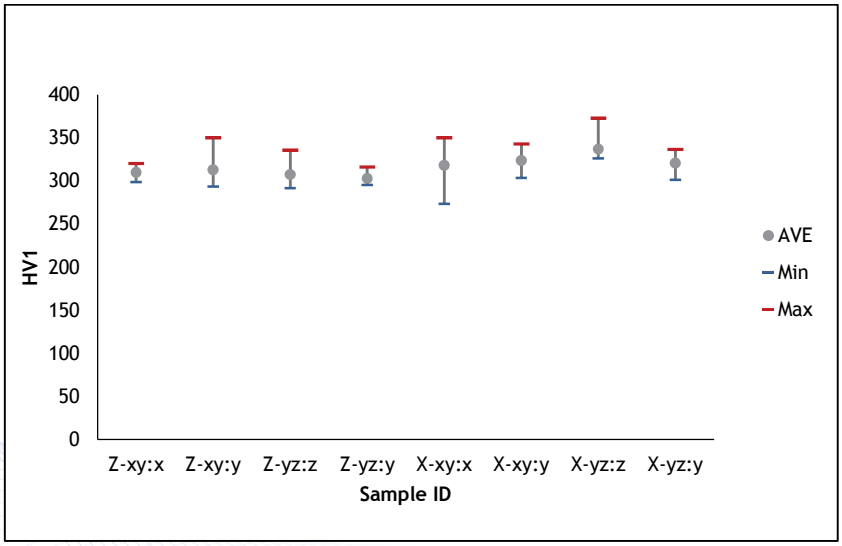

Figure 4: Hardness measurement; Z and X denote building direction and xy & yz are sectioning view; x, y & z are hardness profile measurement *(e.g Z-xy:x; Vertical grown, sectioned in the xy direction and measured in the x-direction)*.

Hardness was conducted to check the variation within the samples; sectioned in both the xy and the yz direction. Data was collected from 6/8 profiles along the reference x, y and z and the results were reported in Figure 4. HV_1 varied with orientation and it also showed homogeneity in the cross sections within the same orientation. Other measured profiles (Z-xy:y; X-xy:x) represented by wide

ISBN 978-0-6398390-0-4

error bars, seemed to be composed of indentations recorded from individual stripes in a layer. Generally, the HV_1 of X samples measured the highest (ΔHV_1 325) than that of Z (ΔHV_1 308) and it also showed the highest variation HV_1 ± 12 (lowest HV_1 273.4 & highest HV_1 372.6) and Z was ± HV_1 5 (lowest HV_1 291.6 & highest HV_1 350).

Tensile tests were conducted on the 25 mm gauge length and 4.4 mm gauge diameter, and the results are tabulated in Table 2. The results resemble those reported in [13]; comparing the effect of heat treatment to the mechanical properties. Tensile properties show similar trends to the hardness profiles. Horizontal samples recorded the higher values (Ys, UTS & *E*) than Z samples. The heights data scattering within the orientation was recorded on the Z samples, with yield strength, Ys ± 15 MPa; while ± 7 MPa was for X samples. Whilst the UTS and elongation was comparative. This results shows improvement on DMLS reproducibility; nonetheless there is still orientation difference of 75 MPa Ys (X_{max} - Z_{min}). The results correspond with the standard for the annealed wrought [4] and they are also common in the Hot isostatic pressing (HIP) products as recorded by [15].

Table 2: Tensile properties

Specimen label	*Ys (Offset 0.2 %) (MPa)*	*E (GPa)*	*UTS (MPa)*	*% Elongation (%)*	*% Reduction of Area*
Z1	827	112	952	15	42
Z2	852	116	960	16	40
Z3	849	115	964	17	43
X1	888	120	968	17	43
X2	893	119	969	16	42
X3	902	121	982	17	45
Ave Z	843±15	114±2	959±6	16±1	42±1
Ave X	895±7	120±1	973±8	16	43±1

Fatigue life properties of Ti6Al4V ELI was investigated on the hour glass polished specimen for high cycle fatigue of 2 000 000 cycles (N). Collected data was reported in Figure 5, presenting the failed and run-out(Nf) specimens. The fatigue life was achieved at 560 MPa (Z) and 600 MPa (X); which is reported by the wrought products as the fatigue limit at very high fatigue cycles (10^8) [16]. The horizontal samples could not gather conclusive data; they show run-out on both the minimum and maximum stresses (560 and 600 MPa). Fatigue failure for Z-type varied from 540 – 650 MPa with increasing N_f value.

Fracrography investigation help understand the mechanism pertaining to the failure. Unlike tensile properties, fatigue is influenced by: 1) crack nucleation and 2) crack propagation. These mechanisms are inclined to the microstructure and the defects in the metal. Crack nucleation in many fatigue failed components is assumed to be due to surface cracks or dirt or porosity if the parts are built via DMLS [7]. The other importance of fractography is to show the mode of failure and also to enlightens on the three regions of fatigue which are crack initiation, stable crack growth and the fast crack area. Crack initiation of most Ti6Al4V originate at the edge of the sample [6, 8, 9, 17]. Whilst the other method; the fish eye is dominant when the surface of the sample has been hardened [18] or the microstructure been duplex (920 °C/1 h + air-cooling and 550 °C/4 h + air-cooling) [19].

Ti6Al4V ELI produced for biomedical implants is mostly heat treated in the vacuum furnace to eliminate the formation of the alpha case, TiO_2 [20] which form during air cooling and influence the mechanical properties negatively.

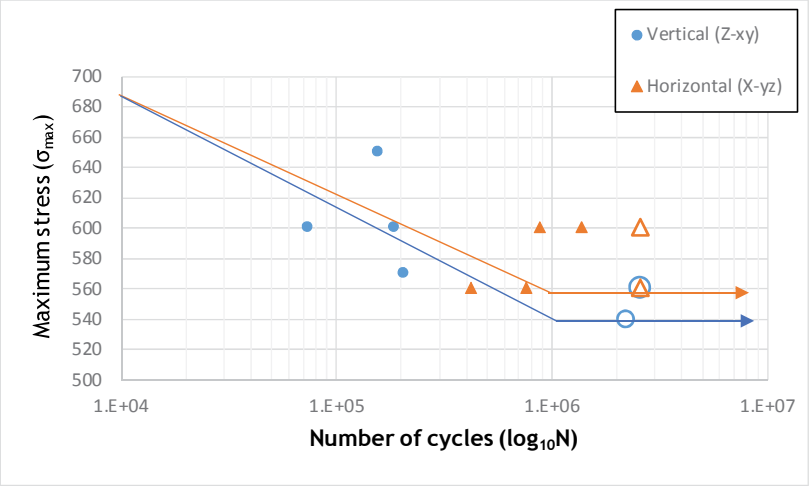

Figure 5: Fatigue properties at frequency of 10 Hz and ratio 0.1.

Defects are not the only driving factor to crack initiation in Ti6Al4V ELI components. Even though fatigue does not induce plastic deformation on the material, it is not exempt for microscopic straining [7]. When a material is subjected to cyclic loading, dislocations are introduced and they are not reversible. This process could act as a form of strengthening mechanism and the more the cycles increases, the dislocations entangle and create microslip onto the surface of the components and eventually the crack initiate [21]. Sometimes in the case of DMLS produced components, the dislocation can meet a pore or un-melted particles which act as stress raisers and there, the crack initiate.

Once the crack nucleated, it becomes easier for the crack to propagate because of the energy on the crack tip [6, 8]. If the surface has a facture and a perpendicular load is applied to the direction of the crack, it grows in relation to the load ratio. With Ti6Al4V ELI, composed of α + ß microstructure, the type of microstructure will influence the crack propagation.

Fractrography of all (Z and X) the failed samples showed that the crack initiated on the surface (Figure 6) [10]. The failure behaviour resembled the standard fatigue stages as shown Figure 1. In Figure 6 (a & b), as pointed by the arrow, the indication of a crack initiation point and region of interest highlighted. The stable crack propagation area, determines the rate at which the crack was growing. It appears to be small for the Z and large for the X type sample, the unstable area is large for the Z and small for the X; also the final fracture is small for the Z and large for the X. Figure 6 (c & d) show the high magnification details of the crack stable crack area.

Dimple structures where observed at high magnification of the stable crack propagation area of the Z samples (Figure 6 c) and fibrous structures were seen on the X samples. The dimple fracture is similar to the structure observed on the unstable or final fracture region [15], while the fibrous is characterized by low values of stress intensity factor. Dimples are associated with bimodal/equiaxed and are praised for superior fatigue resistance, as they promote dislocation slip length [22, 23,24]. A comparison of Z to X type, of the fracture samples with the microstructure suggests that the Figure 6d fracture features correspond to individual α laths.

ISBN 978-0-6398390-0-4

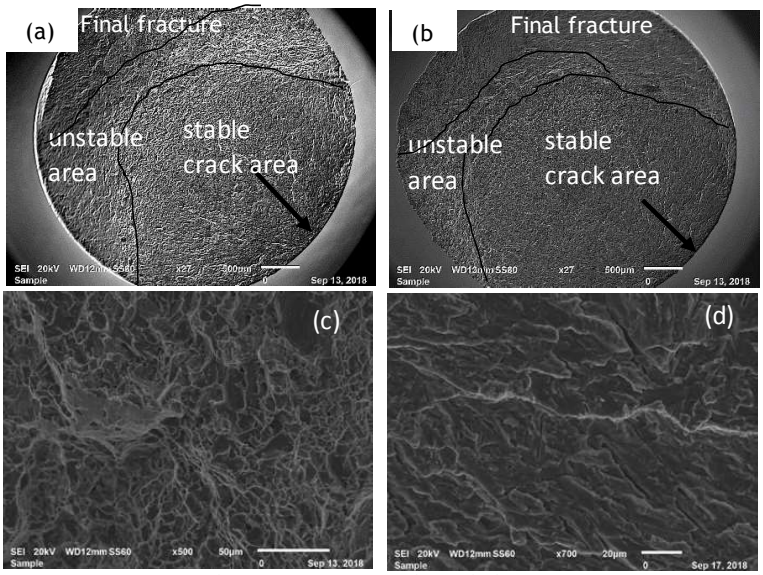

Figure 6: Fatigue fractography; (a) Z grown samples failed at 600 MPa, N*f* 184895 and (b) X grown samples failed at 600 MPa, N*f* 1367868; (c) Z grown high magnification on the stable crack propagation area and (d) X grown high magnification on the stable crack propagation area

Based on the above data, it was obvious that the expected properties of Ti6Al4V ELI are compromised due to the variety in microstructures. As Kumar [24] stated that to improved Ti6Al4V DMLS component properties, post processing to decompose the acicular α' structures from the AM is inevitable. Whilst, the dual alloy could result with either the α/β lamellar, equiaxed or bimodal structures. Consequently, lamella's form via the X-types and the Z-type appeared to describe mixed microstructure; equiaxed. Unfortunately, the two microstructures perceive different fatigue properties. The former is resistant to crack propagation while the latter resist crack initiation during cyclic loading.

CONCLUSION

Investigating microstructure of multidirectional Ti6Al4V from DMLS was done. The alloy was first thermal processed via high-temperature annealing. The aim was to achieve homogenised microstructure; instead lamellar were dominating the X-yz view samples while equiaxed favoured the Z-xy view samples. Hardness was conducted on the same view and an average of X- HV_1 325(± 12) and Z- HV_1 308 (± 5) were recorded. Cup-cone 0.2% offset yield were X- 895 MPa (±7) and 843 MPa (±15) are connected to the lamellar and equiaxed microstructure. The fatigue originated at the edge of the surface; which is common to Ti6Al4V ELI alloys. The orrientations varied with the nature of crack propagation; the Z-dimples and the X- showed fibrous tearing. The better fatigue properties are from the lamellar microstructures because of the α lathes that resist fast crack propagation. The fatigue properties showed a direct relationship to the microstructural and tensile strength.

REFERENCES

[1] **Sonntag, R.** 2015. Fatigue performance of medical Ti6Al4V alloy after mechanical surface treatments, *PloS one*, *10*(3), p.e0121963.

[2] Liang, H. 2004. Applications of plasma coatings in artificial joints: an overview, *Vacuum*, *73*(3-4), pp.317-326.
[3] Colic, K. 2017. Experimental and numerical research of mechanical behavior of titanium alloy hip implant, *Tehnički vjesnik-Technical Gazette*, 24(3), pp.709-713.
[4] de Formanoir, C. 2017. A strategy to improve the work-hardening behavior of Ti-6Al-4V parts produced by additive manufacturing, *Materials Research Letters*, 5(3), pp.201-208.
[5] Fan, Y. 2016. Relationships among the microstructure, mechanical properties, and fatigue behavior in thin Ti6Al4V, *Advances in materials science and engineering*.
[6] Hosseini, S., 2012. Fatigue of Ti-6Al-4V. *Biomedical Engineering-Technical Applications in Medicine*, pp.75-92. IntechOpen'
[7] Tu, S. T. 2016. Fatigue crack initiation mechanisms. *Reference Module in Materials Science and Materials Engineering*, 2016, Pp.1-23.
[8] Bridier, F. 2008. Slip and fatigue crack formation processes in an α/β titanium alloy in relation to crystallographic texture on different scales. *Acta Materialia*, *56*(15), pp.3951-3962.
[9] Malefane, L. B. 2018. Tensile and high cycle fatigue properties of annealed Ti6Al4V (ELI) specimens produced by direct metal laser sintering. *South African Journal of Industrial Engineering*, *29*(3), pp.299-311.
[10] ASTM standard. ASM Handbook, Volume 11 - Failure Analysis and Prevention
[11] Thejane, K. 2016, November. Characterisation of Ti6Al4V (ELI) powder used by the South Aftrican Collaborative Program in Additive Manufacturing. In *Proceedings of the 17th Annual International RAPDASA Conference*, pp.2-6.
[12] Mengucci, P. 2017. Effects of build orientation and element partitioning on microstructure and mechanical properties of biomedical Ti-6Al-4V alloy produced by laser sintering. *Journal of the mechanical behavior of biomedical materials*, *71*, pp.1-9.
Moletsane, M.G. 2016. *Microstructure and mechanical properties of Ti6Al4V (ELI) parts produced by DMLS* (Doctoral dissertation, Bloemfontein: Central University of Technology, Free State).
[13] ASTM standards. 2014. ASTM 1472-14 Standard Specification for Wrought Titanium-6Aluminum-4Vanadium Alloy for Surgical Implant Applications (UNS R56400)
[14] Becker, T.H. 2015. Microstructure and mechanical properties of direct metal laser sintered Ti-6Al-4V, *South African Journal of Industrial Engineering*, *26*(1), pp.1-10.
[15] Janeček, M. 2015. The Very High Cycle Fatigue Behaviour of Ti-6Al-4V Alloy. *Acta Physica Polonica, A.*, *128*(4).
[16] Pan, X. 2019. High-cycle and very-high-cycle fatigue behaviour of a titanium alloy with equiaxed microstructure under different mean stresses. *Fatigue & Fracture of Engineering Materials & Structures*.
[17] Su, H. 2017. Nanograin layer formation at crack initiation region for very-high-cycle fatigue of a Ti-6Al-4V alloy, *Fatigue & Fracture of Engineering Materials & Structures*, *40*(6), pp.979-993.
[18] Everaerts, J. 2016. Internal fatigue crack initiation in drawn Ti-6Al-4V wires, *Materials Science and Technology*, *32*(16), pp.1639-1645.
[19] Mohite, N. 2017, December. Development and Removal of Alpha-Case Layer from Heat Treated Titanium Alloys. In *ASME 2017 Gas Turbine India Conference* (pp. V002T10A011-V002T10A011). American Society of Mechanical Engineers.
[20] Sangid, M. D. 2013. The physics of fatigue crack initiation. *International journal of fatigue*, *57*, pp.58-72.
[21] Pilchak, A. L. 2009. The effect of microstructure on fatigue crack initiation in Ti-6Al-4V. In ICF12, Ottawa 2009.
[22] Benedetti, M. 2018. Low-and high-cycle fatigue resistance of Ti-6Al-4V ELI additively manufactured via selective laser melting: Mean stress and defect sensitivity, International Journal of Fatigue, 107, pp.96-109.
[23] Kumar, P. 2019. Microstructural optimization through heat treatment for enhancing the fracture toughness and fatigue crack growth resistance of selective laser melted Ti-6Al-4V alloy, *Acta Materialia*, pp.45-59.

ISBN 978-0-6398390-0-4